Improved Oxidative C−C Bond Formation Reactivity of High-Valent Pd Complexes Supported by a Pseudo-Tridentate Ligand

Jason W. Schultz, Nigam P. Rath, and Liviu M. Mirica*

ACCESS | 📊 Metrics & More | 📖 Article Recommendations | 🔵 Supporting Information

ABSTRACT: There is a large interest in developing oxidative transformations catalyzed by palladium complexes that employ environmentally friendly and economical oxidizing reagents such as dioxygen. Recently, we have reported the isolation and characterization of various mononuclear Pd^{III} and Pd^{IV} complexes supported by the tetradentate ligands N,N'-dialkyl-2,11-diaza[3.3](2,6)-pyridinophane ($^RN4$, R = ^tBu, ^iPr, Me), and the aerobically induced C−C and C-heteroatom bond formation reactivity was investigated in detail. Given that the steric and electronic properties of the multidentate ligands were shown to tune the stability and reactivity of the corresponding high-valent Pd complexes, herein we report the use of an asymmetric N4 ligand, N-mehtyl-N'-tosyl-2,11-diaza[3.3]-(2,6)pyridinophane ($^{TsMe}N4$), in which one amine N atom contains a tosyl group. The N-Ts donor atom exhibits a markedly reduced donating ability, which led to the formation of transiently stable Pd^{III} and Pd^{IV} complexes, and consequently the corresponding O_2 oxidation reactivity and the subsequent C−C bond formation were improved significantly.
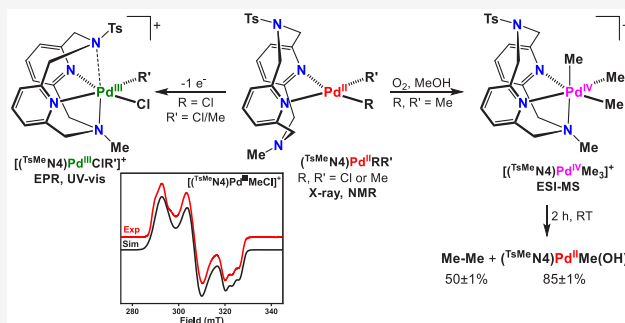

INTRODUCTION

Aerobic transformations catalyzed by palladium complexes are a growing synthetic method that provides a practical use of dioxygen as an environmentally benign and inexpensive oxidant for a range of oxidative organic transformations.[1−8] The majority of the reported transformations involve a $Pd^{0/II}$ catalytic cycle in which dioxygen regenerates the Pd^{II} species. However, recently an increasing number of high-valent Pd^{IV} and/or Pd^{III} active intermediates have been reported in several catalytic and stoichiometric aerobic transformations.[9−17]

We have recently reported several $Pd^{II}Me_2$ complexes supported by tetradentate ligands N,N'-dialkyl-2,11-diaza[3.3]-(2,6)pyridinophane ($^RN4$, R = ^tBu, ^iPr, Me) that are capable of undergoing facile oxidation by O_2 or peroxides to produce Pd^{III} and Pd^{IV} intermediates, which undergo elimination of ethane under ambient conditions (Scheme 1).[18,19] Similarly, we have reported the aerobic oxidation of $(Me_3tcan)Pd^{II}Me_2$ (Me_3tacn = N,N',N''-trimethyl-1,4,7-triazacyclononane) to produce a stable high-valent Pd^{IV} complex $[(Me_3tacn)Pd^{IV}Me_3]^+$

Scheme 1. Reported Aerobic Reactivity of $(^{tBu}N4)PdMe_2$[18] and $(^{Me}N4)PdMe_2$[19]
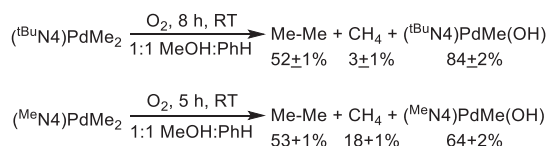
(Scheme 2), which can undergo reductive elimination of ethane at elevated temperatures.[20] In all these studies, the

### Scheme 2. Reported Aerobic Reactivity of $(Me_3tacn)PdMe_2$[20]
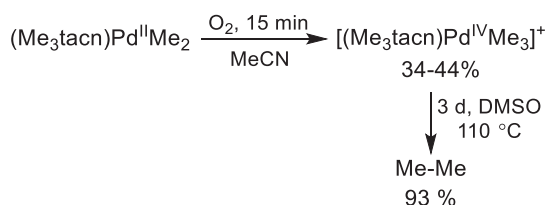
stability of the high-valent Pd species has been shown to be essential in controlling the subsequent C−C bond formation reactivity.[21,22]

In the case of the $(^RN4)PdMe_2$ complexes, it was proposed that the increased stability of the Pd^{III} and Pd^{IV} intermediates leads to a slower C−C bond formation reactivity. For the $(^{Me}N4)PdMe_2$ system, the Pd^{IV} species $[(Me_3tacn)Pd^{IV}Me_3]^+$ was observed to form during aerobic oxidation in up to 34%

yield,[19] and its decay correlated to the formation with ethane over several hours, along with formation of methane as a side product in 18% yield. Similarly, in the case of the tridentate ligand Me₃tcan, the corresponding $[(Me_3tacn)Pd^{IV}Me_3]^+$ complex was found to be stable indefinitely at room temperature, which leads to a dramatically diminished rate of C−C bond formation that occurred only at elevated temperatures (Scheme 2).[20] Therefore, one could imagine an increased reactivity when these high-valent Pd intermediates are destabilized through carefully designed ligand modifications. Herein, we report the synthesis and reactivity of Pd[II] complexes supported the ligand *N*-mehtyl-*N′*-tosyl-2,11-diaza-[3.3](2,6)pyridinophane (^{TsMe}N4), in which one amine group has a tosyl substituent (Scheme 3).[23−25] Given the limited

Scheme 3. Structural Comparison of Previously Synthesized N4 Ligands (^{R}N4) and the Newly Modified Pseudo-Tridentate Variant (^{TsMe}N4)
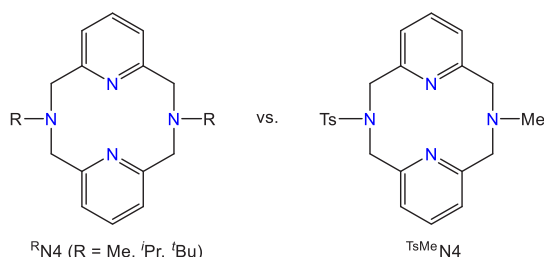

donating ability of an N-tosylated amine, we propose that ^{TsMe}N4 could act as a pseudo-tridentate ligand in which the N-Ts donor atom interacts only weakly with the Pd center. Indeed, the pseudo-tridentate nature of the ^{TsMe}N4 was experimentally confirmed using electron paramagnetic resonance (EPR) spectroscopy. Interestingly, this ligand was still able to stabilize high-valent Pd species, albeit to a lesser extent. As a result, the aerobic oxidation of the corresponding Pd[II]Me₂ complex proceeds directly to the key $[(^{TsMe}N4)Pd^{IV}Me_3]^+$ intermediate—without the formation of an appreciable amount of the $[(^{TsMe}N4)Pd^{III}Me_2]^+$ species, followed by a more rapid decay to generate the C−C bond formation product ethane in stoichiometric yields in 2 h at room temperature and with no formation of methane or other side products. Overall, these results suggest that altering the electron donating ability of the donor atoms as well as the denticity of the multidentate ligand employed can finely tune the oxidatively induced reactivity of high-valent Pd complexes. It is important to note that the steric influence of the N-substituents of pyridinophane ligands on the corresponding metal complexes has been reported previously by us and other groups for Pd,[26−28] Ni,[29−31] and Mn[32] complexes. In addition, the effect of electron donating ability of the amine donors in the pyridinophane ligands has also been reported recently by our group for Ni complexes;[24,25] however, no such electron donating ability effects have been reported for Pd complexes.

■ **RESULTS AND DISCUSSION**

Ligand Design and Synthesis. The *N*-methyl-*N′*-tosyl-2,11-diaza[3.3](2,6)pyridinophane (^{TsMe}N4) ligand is a variant of the previously studied tetradentate ligands, *N,N′*-di-*tert*-butyl-2,11-diaza[3.3](2,6)pyridinophane (^{tBu}N4),[33] *N,N′*-di-methyl-2,11-diaza[3.3](2,6)pyridinophane (^{Me}N4), and *N,N′*-di-*iso*-propyl-2,11-diaza[3.3](2,6)pyridinophane (^{iPr}N4).[19] The

^{TsMe}N4 ligand was designed to behave like a pseudo-tridentate ligand by attaching a bulky electron-withdrawing protecting group to one of the axial amines in order to alter the metal-binding ability of that N donor atom.[24,25] ^{TsMe}N4 was successfully synthesized by a new synthetic route (Scheme

Scheme 4. Synthetic Route for the Pseudo-Tridentate ^{TsMe}N4
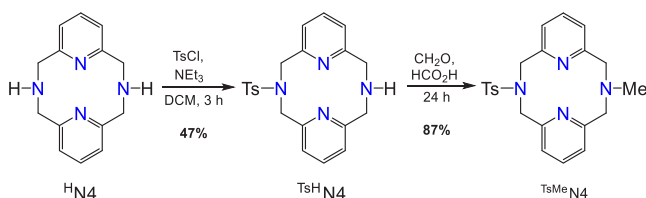
4) that started with the preparation of the new intermediate, ^{TsH}N4, which was prepared in 47% yield via selective monotosylation of the ^{H}N4 precursor[34] using 4-toluenesulfonyl chloride.[23] The ^{TsH}N4 intermediate was then methylated using Eschweiler-Clarke conditions to produce the desired ligand, ^{TsMe}N4, in 87% yield.

Synthesis and Characterization of (^{TsMe}N4)Pd[II] Complexes. The Pd[II] complexes (^{TsMe}N4)PdCl₂ (**1**), (^{TsMe}N4)-PdMeCl (**2**), and (^{TsMe}N4)PdMe₂ (**3**) were obtained in a manner similar to the previously synthesized ^{R}N4 analogues (Scheme 5).[18,19,35] Complex **1** was prepared in 86% yield from

Scheme 5. Synthesis of (^{TsMe}N4)Pd[II]/Pd[III] Complexes
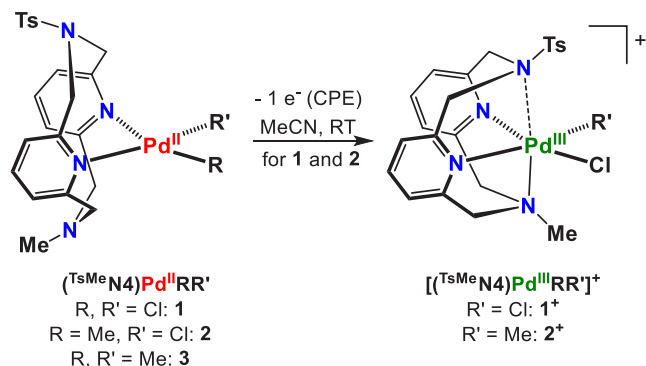
the precursor (COD)Pd[II]Cl₂[36] via ligand exchange with ^{TsMe}N4. Similarly, complexes **2** and **3** were prepared in 84% and 59% yields from the precursors (COD)Pd[II]MeCl[37] and (COD)Pd[II]Me₂,[18] respectively.

The X-ray structure of **1** reveals a unique square planar geometry around the Pd[II] metal center, with two chloride ligands, the N-Me amine donor, and one pyridine N atom of the ^{TsMe}N4 ligand binding in the equatorial plane (Figure 1). This unique bonding geometry is different from the previously synthesized (^{R}N4)Pd[II] complexes, in which a square planar geometry involving the two exogenous ligands and the two pyridine N atoms is usually observed. However, the metrical parameters of complex **1** are comparable to those of the previously synthesized complexes (^{tBu}N4)PdCl₂ and (^{Me}N4)-PdCl₂.[15,16,33]

The X-ray structures of complexes **2** and **3** reveal that both complexes adopt the more commonly observed bonding geometry featuring both the pyridine N atoms bound to the
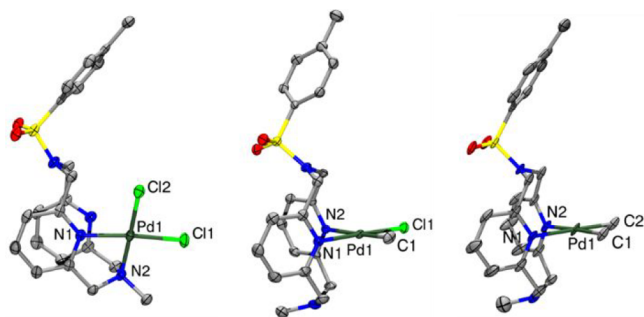
Figure 1. ORTEP representation (50% probability ellipsoids) of **1** (left), **2** (middle), and **3** (right). Selected bond distances (Å): **1**, Pd1−Cl1 2.2792(9), Pd1−Cl2 2.3065(8), Pd1−N1 2.057(2), Pd1−N2 2.062(3); **2**, Pd1−C1 2.027(2), Pd1−Cl1 2.3073(6), Pd1−N1 2.044(2), Pd1−N2 2.1724(19); **3**, Pd1−C1 2.053(7), Pd1−C2 2.053(7), Pd1−N1 2.151(6), Pd1−N2 2.151(6).

Pd metal center (Figure 1). Additionally, the metrical parameters of complexes **2** and **3** are also comparable to those of the corresponding previously synthesized Pd complexes, as well as to the recently reported (^{TsMe}N4)NiMe$_2$ complex.[25]

Cyclic voltammetry of all three Pd^{II} complexes in 0.1 M Bu$_4$NClO$_4$ in CH$_2$Cl$_2$ or THF reveals a series of oxidation waves over a wide range of potentials (Figure 2 and Table 1). The cyclic voltammogram (CV) of **1** reveals oxidation peaks at 715 and 950 mV and a reversible wave at 1100 mV vs Fc$^+$/Fc. Similarly, the CV of **3** exhibits two oxidation peaks and a reversible wave at −440, −130, and 73.4 mV vs Fc$^+$/Fc, respectfully. The CV of **2**, however, reveals a single oxidation wave at 100 mV and a reversible wave at 605 mV vs Fc$^+$/Fc. Since the ^{TsMe}N4 ligand is not redox active within this potential range, the irreversible oxidations peaks are assigned to the Pd$^{II/III}$ oxidation events corresponding to the two conformations in which ^{TsMe}N4 adopts a κ^3 or κ^4 binding mode, respectively, while the reversible oxidation wave is assigned to the Pd$^{III/IV}$ redox cycle. These assignments are consistent with our previously reported detailed electrochemical analyses of various (^{R}N4)Pd complexes.[35,38] The observed oxidation potentials of **1**−**3** are slightly higher than the previously synthesized complexes,[18,19,35] likely due to both the electron withdrawing and the steric effect of the N-tosyl group that stabilizes to a lesser extent the high-valent Pd centers.

Synthesis and Characterization of (^{TsMe}N4)Pd^{III} Complexes. Controlled potential electrolysis (CPE) of **1** and **2** at potentials above the first anodic wave were performed to generate deeply colored solutions of complexes [(^{TsMe}N4)-Pd^{III}Cl$_2$]$^+$ (**1$^+$**, forest green) and [(^{TsMe}N4)Pd^{III}MeCl]$^+$ (**2$^+$**, purple). The UV−vis spectra of **1$^+$** and **2$^+$** in MeCN show strong absorption bands at 545−665 nm and 350−380 nm (Figure 3). Additionally, the reduced stability of the Pd^{III} complexes was also monitored via UV−vis spectroscopy. The characteristic Pd^{III} absorption bands for complexes **1$^+$** and **2$^+$** decay at room temperature within 30 min and 2 h, respectively, which is in contrast to the much more stable analogous (^{R}N4)Pd^{III} complexes (R = Me, iPr, tBu).[15,16,33] Moreover, neither electrochemical nor chemical oxidation of **3** was capable of producing detectable amounts of the corresponding Pd^{III} product **3$^+$**, and thus supporting our hypothesis that the pseudo-tridentate nature of the ^{TsMe}N4 ligand results in the marked destabilization of the Pd^{III} centers.
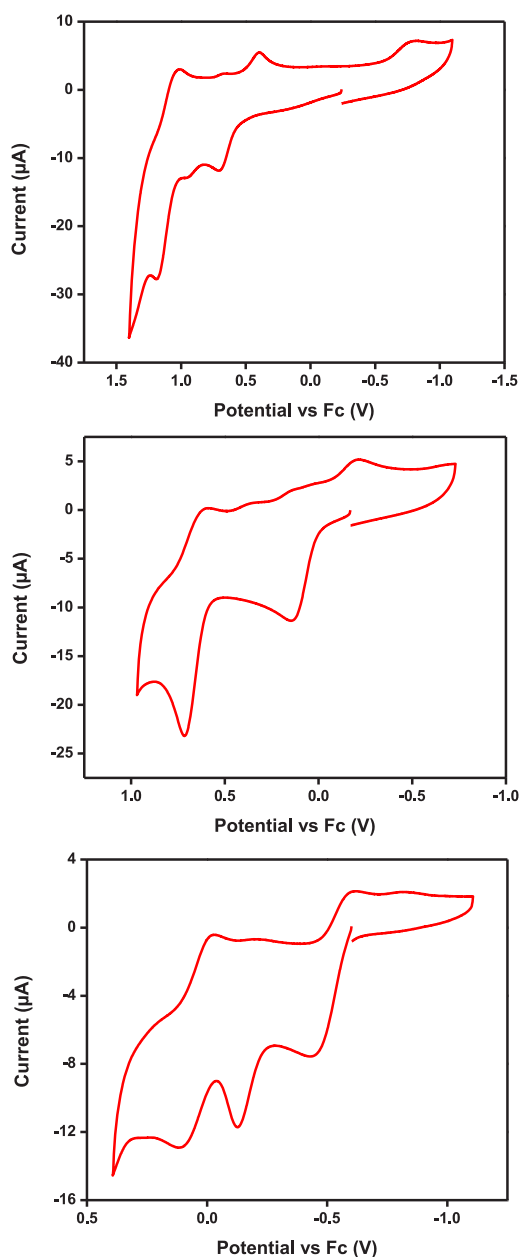
Figure 2. Cyclic voltammograms of **1** (top), **2** (middle), and **3** (bottom) in 0.1 M Bu$_4$NClO$_4$ in CH$_2$Cl$_2$ (for **1** and **2**) or THF (for **3**), 100 mV/s scan rate.

Table 1. Redox Potentials of Complexes 1, 2, and 3[a]

complex	E_{pa}(Pd$^{II/III}$) (mV)	E_{pc}(Pd$^{III/II}$) (mV)	$E_{1/2}$(Pd$^{III/IV}$) (mV)
1	715, 950	670, 396	1100
2	100	−45, −220	605
3	−440, −130	−615	74

[a]Measured vs Fc$^+$/Fc in 0.1 M Bu$_4$NClO$_4$ in CH$_2$Cl$_2$ (for **1** and **2**) or THF (for **3**), at 100 mV/s scan rate.

Complexes **1$^+$** and **2$^+$** are both paramagnetic, allowing the bonding interactions with the Pd metal center to be probed using electron paramagnetic resonance spectroscopy (EPR). The EPR spectra of **1$^+$** and **2$^+$** (in 3:1 PrCN/MeCN frozen glass at 77 K) reveals that the two axial amino donors interact to a different extent with the Pd^{III} center, in contrast to the
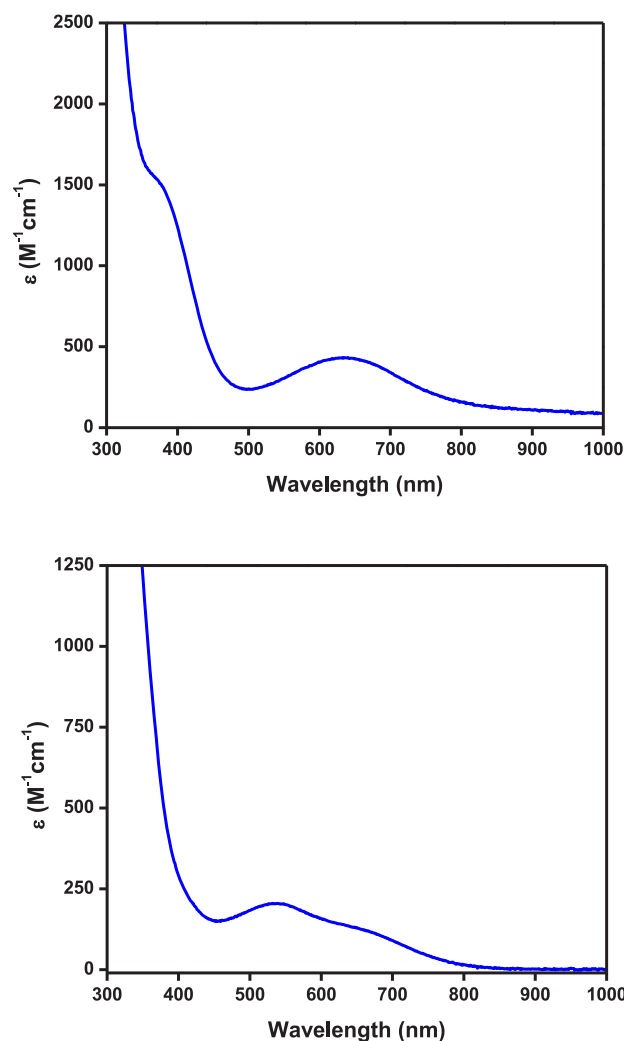
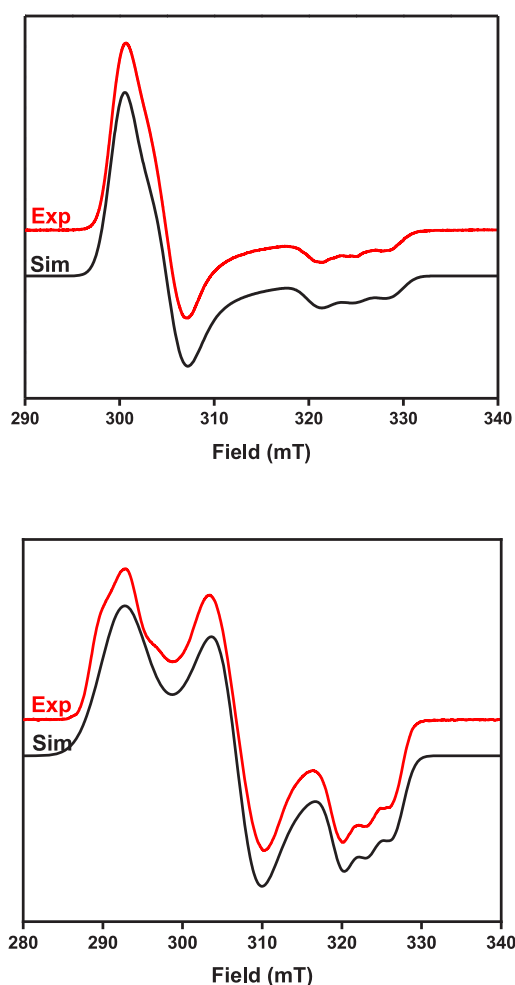**Figure 3.** UV−vis spectra of $[1^+]ClO_4$ (0.5 mM, top) and $[2^+]ClO_4$ (1 mM, bottom) in MeCN.

Figure 4. EPR spectra of a solution of $[1^+]ClO_4$ (top) and $[2^+]ClO_4$ (bottom) in a 3:1 PrCN/MeCN frozen glass at 77 K (red lines), and simulated EPR spectra (black lines). The following parameters were used for the simulations: $[1^+]ClO_4$, g_x = 2.1632, g_y = 2.1290, g_z = 2.0005 (A_{N1} = 35.5 G, A_{N2} = 10.0 G); $[2^+]ClO_4$, g_x = 2.2220, g_y = 2.1180, g_z = 2.0110 (A_{N1} = 31.5 G, A_{N2} = 5.0 G).

previously reported Pd^{III} complexes supported by the symmetric $^RN4$ ligands (Figure 4).[3,4,12]

For complex 1^+ the Pd^{III} center strongly couples to the N atom of the N-Me group ($A_{z(N1)}$ = 35.5 G) and weakly couples to the N atom of the N-Ts group ($A_{z(N2)}$ = 10.0 G) in the g_z direction. This variance in the N atom superhyperfine coupling constants produces a distinctive coupling pattern observed in the EPR spectrum, in which the weakly coupled N atom of the N-Ts group leads to a broadening on the superhyperfine coupling pattern of the N atom of the N-Ts group, resulting in the observed broadened "triplet of triplets" (Figure 4). In addition, for complex 2^+ the coupling between the Pd metal center and the N of the N-Ts group amine is even less ($A_{z(N2)}$ = 5.0 G), given the presence of the stronger methyl ligand donor, and as a result the broadening of the observed superhyperfine coupling in the g_z direction is reduced (Figure 4). Similar coupling patterns in the in the g_z direction have been observed recently by us for the related organometallic Ni^{III} complexes supported by the $^{TsMe}N4$ ligand.[24,25]

These distinctly different superhyperfine coupling constants for the N-Me and N-Ts donating groups strongly support the proposed pseudo-tridentate nature of the $^{TsMe}N4$ ligand. Furthermore, the extent to which the N atoms of the N-Me and N-Ts group couple with the Pd^{III} center appears to be

dependent on the exogenous ligands bonded to Pd. The more σ-donating the exogenous ligands (that is methyl vs chloride ligands), the weaker the interactions between the Pd center and the axial N-Ts and N-Me groups, resulting in weaker superhyperfine coupling in the g_z direction. From this general trend, the binding coordination of $^{TsMe}N4$ in the $Pd^{III}Me_2$ complex 3^+ is proposed to be almost completely tridentate, and thus leading to the marked instability of 3^+ (vide infra).

Computational Studies of Complexes 1^+ and 2^+. Because of the low stability of complexes 1^+ and 2^+, X-ray quality crystals of these complexes could not be isolated. However, it is evident from the above spectroscopic studies that complexes 1^+ and 2^+ are formed in solution. Furthermore, the resulting EPR results suggest the bonding geometry around the Pd^{III} center is based on the pseudo-tridentate nature of the $^{TsMe}N4$ ligand (Figure 4). To support the proposed structures, density functional theory (DFT) and time-dependent density functional theory (TD-DFT) calculations were performed, and the resulting metrical parameters for the optimized geometries of 1^+ and 2^+ were compared to the previously characterized $^{Me}N4$-supported complexes $[(^{Me}N4)Pd^{III}Cl_2]^+$ (4^+) and $[(^{Me}N4)Pd^{III}MeCl]^+$ (5^+, Table 2). The bond distances for

Table 2. DFT-Calculated (UB3LYP/CEP-31G) Metrical Parameters for Complexes 1⁺ and 2⁺ Compared to the DFT-Calculated Values[a] for Similar ^{Me}N4-Supported Complexes 4⁺ and 5⁺

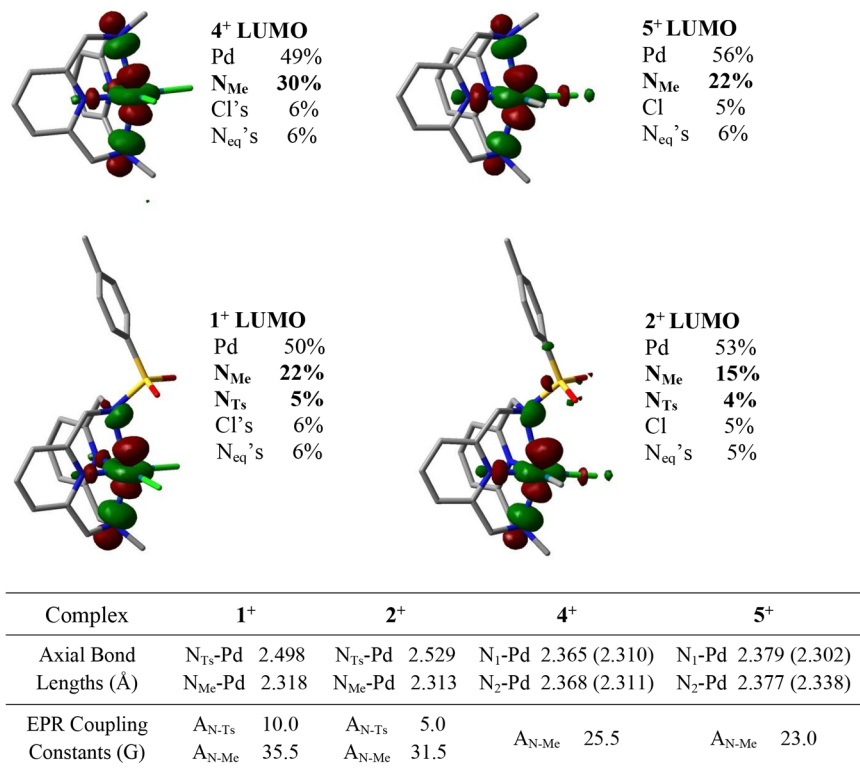| metrical parameters	1⁺ DFT	4⁺ DFT (Expt)	2⁺ DFT	5⁺ DFT (Expt)
		Bond Lengths		
Pd−N1(Ts/Me)	2.498	2.365 (2.310)	2.529	2.379 (2.302)
Pd−N2 (Me)	2.318	2.368 (2.311)	2.313	2.377 (2.338)
Pd−N3 (Py)	2.063	2.051 (2.029)	2.111	2.104 (2.085)
Pd−N4 (Py)	2.067	2.052 (2.002)	2.181	2.148 (2.085)
Pd−Cl1	2.416	2.425 (2.303)	2.466	2.486 (2.344)
Pd−Cl2/C1	2.417	2.424 (2.322)	2.073	2.070 (2.021)
		Bond Angles		
N1−Pd−N2	150.6	153.3 (153.5)	146.5	149.7 (149.1)
N3−Pd−N4	82.8	83.2 (82.3)	80.9	81.5 (81.4)

[a]X-ray experimental parameters shown in parentheses.

the axial N atoms in 4⁺ and 5⁺ were determined to be symmetric, whereas in 1⁺ and 2⁺ the bond distances are clearly different between the N-Me and N-Ts N atoms, with the electron-deficient N-Ts N atom being unable to form a strong interaction with the Pd^{III} center. In addition, the DFT-calculated metrical parameters for complexes 1⁺ and 2⁺ correlate well with the experimental EPR results (Figure 5). The less σ-donating the exogenous ligands (that is chloride vs methyl ligands), the longer the calculated distances between Pd center and the axial N-Ts and N-Me groups and in line with weaker superhyperfine couplings in the g_z direction. Moreover, the calculated N_{axial} atomic contributions to the LUMO's for 1⁺ and 2⁺ show that the N-Me donor atoms interact more

strongly with the Pd^{III} center then the N-Me donor atoms in 4⁺ and 5⁺, while the N-Ts donor atoms interact more weakly (Figure 5).

Furthermore, TD-DFT calculations were employed to simulate the UV/vis spectra for complexes 1⁺ and 2⁺ (Figure 6).[39] Excitingly, the calculated UV−vis spectra match very well the experimental spectra, strongly supporting the calculated optimized geometries for 1⁺ and 2⁺, and most importantly validating their calculated electronic properties.

Aerobic Reactivity of (^{TsMe}N4)Pd^{II}Me₂ (3). On account of the low oxidation potential observed for complex 3, as well as the previously observed aerobic oxidation of (^{tBu}N4)Pd^{II}Me₂ and (^{Me}N4)Pd^{II}Me₂,[18,19] we proposed that 3 could be similarly oxidized using mild oxidants to form reactive high-valent Pd species. Therefore, a solution of 3 in MeOH was reacted with O₂, and the reaction was monitored by NMR to reveal the formation of ethane in up to 50% yield (Scheme 6). This yield is similar to the results previously reported for the other (^{R}N4)Pd^{II}Me₂ complexes; however, no methane side product was obtained even though the reaction was performed in a protic solvent, and the reaction was already complete in 2 h.[18,19] Furthermore, the observed C−C bond formation reactivity was not affected by the presence of the alkyl radical trap TEMPO, suggesting a nonradical mechanism.[39] Finally, the reaction of 3 with MeI gave ethane in 89% and 99% yields when 1 equiv or 20 equiv of MeI were used, respectively, suggesting a rapid oxidative addition to generate a [(^{TsMe}N4)-Pd^{IV}Me₃]⁺ intermediate,[40−46] followed by C−C reductive eliminate to form ethane (Scheme 7).

Detection of High-Valent Pd Intermediates. In the previously reported cases, the formation of [(^{R}N4)Pd^{III}Me₂]⁺

| Complex	1⁺		2⁺		4⁺	5⁺
Axial Bond Lengths (Å)	N_{Ts}-Pd 2.498		N_{Ts}-Pd 2.529		N_1-Pd 2.365 (2.310)	N_1-Pd 2.379 (2.302)
	N_{Me}-Pd 2.318		N_{Me}-Pd 2.313		N_2-Pd 2.368 (2.311)	N_2-Pd 2.377 (2.338)
EPR Coupling Constants (G)	A_{N-Ts} 10.0		A_{N-Ts} 5.0		A_{N-Me} 25.5	A_{N-Me} 23.0
	A_{N-Me} 35.5		A_{N-Me} 31.5			

Figure 5. DFT-calculated (UB3LYP/CEP-31G) molecular orbitals (β LUMOs) of 1⁺ (bottom-left) and 2⁺ (bottom-right) compared to the ^{Me}N4-supported complexes 4⁺ (top-left) and 5⁺ (top-right), and the calculated atomic contributions, DFT-calculated (and X-ray experimental values) Pd−N_{axial} bond distances, and the experimental EPR superhyperfine coupling constants.
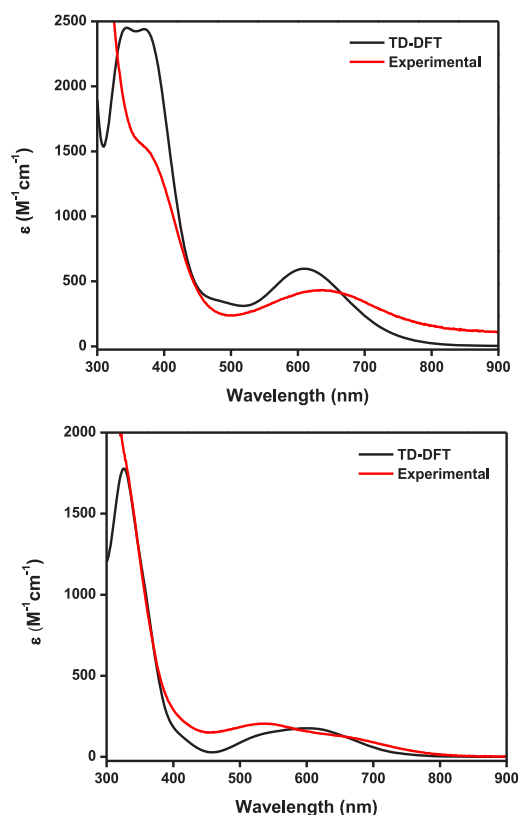
Figure 6. Comparison of experimental (red line) and computational simulated (black line) UV−vis spectra of complexes $[\mathbf{1^+}]\mathrm{ClO_4}$ (top) and $[\mathbf{2^+}]\mathrm{ClO_4}$ (bottom) in MeCN.

Scheme 6. C−C Bond Formation Reactivity of $(^{\mathrm{TsMe}}\mathrm{N4})\mathrm{Pd^{II}Me_2}$ (3)
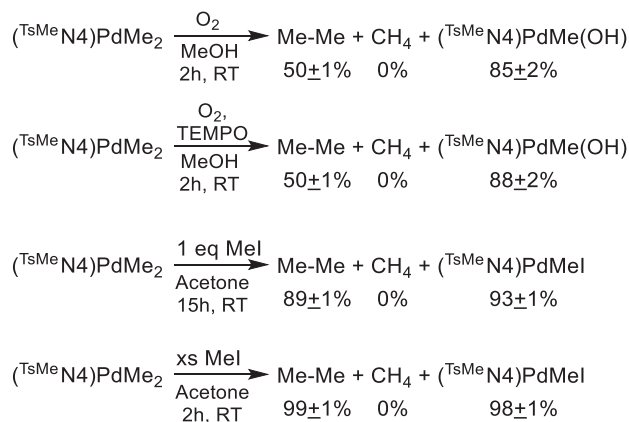
species upon aerobic oxidation was monitored by UV−vis spectroscopy and confirmed by EPR and ESI-MS.[18,19] In the case of complex $\mathbf{3^+}$, monitoring its reaction with O_2 by UV−vis in MeOH did not reveal the formation of any intermediate species with a characteristic absorption spectrum, and the reaction progressed directly from the starting material to the final product (Figure 7). Since a Pd^{III} species would be expected to be colored,[18,19] this further supports our assumption that the pseudo-tridentate $^{\mathrm{TsMe}}\mathrm{N4}$ ligand does not stabilize the Pd^{III} center to a great extent, and thus leads to an increased C−C bond formation reactivity.

Similarly, the formation of any Pd^{III} intermediate was not observed when the aerobic reaction mixture was analyzed by

EPR spectroscopy at different time points. However, a trace amount of the $[(^{\mathrm{TsMe}}\mathrm{N4})\mathrm{Pd^{III}Me_2}]^+$ species $\mathbf{3^+}$ was observed by ESI-MS, which reveals a peak at m/z 545.1131 (calculated for $\mathbf{3^+}$: 544.1124). Species $\mathbf{3^+}$ is formed within the first minute after the start of the aerobic oxidation; however, it fully decays within 10 min to the key intermediate $[(^{\mathrm{TsMe}}\mathrm{N4})\mathrm{Pd^{IV}Me_3}]^+$, **4**. The lifetime of **4** is much longer, and its presence is confirmed by ESI-MS until the completion of the reaction. These results suggest the direct formation of the key Pd^{IV} intermediate **4** without progressing through the Pd^{III} intermediate $\mathbf{3^+}$. Additionally, the observed rate of ethane formation is slightly larger than that for the previously reported $(^{R}\mathrm{N4})\mathrm{Pd^{II}Me_2}$ complexes (R = tBu, iPr, Me),[15,16] suggesting that the N-Ts donor arm of $^{\mathrm{TsMe}}\mathrm{N4}$ in the $[(^{\mathrm{TsMe}}\mathrm{N4})\mathrm{Pd^{IV}Me_3}]^+$ species **4** may further destabilize it, possibly by distorting the octahedral coordination of the Pd^{IV} center and thus promoting the C−C reductive elimination step.

Proposed Mechanism for the Aerobic C−C Bond Formation Reactivity of 3. On the basis of the experimental results described above, and by analogy with the aerobic oxidation of previously reported Pt^{II}-dimethyl and Pd^{II}-dimethyl complexes,[47−49] we propose a mechanism for the aerobically induced C−C bond formation from **3** that is slightly altered from the previously reported mechanisms for $(^{tBu}\mathrm{N4})\mathrm{Pd^{II}Me_2}$ and $(^{Me}\mathrm{N4})\mathrm{Pd^{II}Me_2}$,[18,19] in which the key intermediate **4** is generated without going through the $\mathbf{3^+}$ intermediate (Scheme 7). Oxidation of **3** by O_2 through an inner-sphere mechanism is expected to generate a transient Pd^{III}-superoxide intermediate, $[(\kappa^3\text{-}^{\mathrm{TsMe}}\mathrm{N4})\mathrm{Pd^{III}Me_2(O_2)}]$.[15,16] The direct oxidation of **3** by O_2 is supported by its low Pd^{II}/Pd^{III} oxidation potential, which is similar to that of the $(^{tBu}\mathrm{N4})\mathrm{Pd^{II}Me_2}$ complex that can reduce O_2 electrocatalytically.[18] Upon protonation, this would yield the Pd^{IV}(hydroperoxo) species **6**, which was detected transiently via ESI-MS during the aerobic oxidation.[39] The intermediate species **6** can then oxidize another molecule of **3** to give two molecules of the Pd^{IV}(hydroxo) species **7**, which can then undergo a Pd^{IV}-to-Pd^{II} methyl group transfer with complex **3** to produce the key reactive intermediate **4** and the final Pd^{II}methyl(hydroxo) product **5**. The key $[(^{\mathrm{TsMe}}\mathrm{N4})\mathrm{Pd^{IV}Me_3}]^+$ intermediate **4** would then undergo the rate-determining reductive elimination of ethane along with another equivalent of the Pd^{II} product **5** (Scheme 7). The reductive elimination of ethane via intermediate **4** was independently confirmed via the observed reactivity of MeI with complex **3**, to give directly ethane in up to 99% yield in 2 h (Scheme 6).[39] While the proposed mechanism does not include any dinuclear Pd intermediate species since the TsMeN4 ligand is considered to be fairly sterically bulky, we cannot completely rule out the possibility of dinuclear $Pd^{II}-Pd^{IV}$ or $Pd^{III}-Pd^{III}$ species formed during this aerobically induced ethane formation process.[50]

■ **CONCLUSION**

In summary, reported herein is the synthesis, characterization, and reactivity of a series of Pd^{II} complexes supported by a pseudo-tridentate $^{\mathrm{TsMe}}\mathrm{N4}$ asymmetric pyridinophane ligand, in which one amine N atom contains a tosyl group. The pseudo-tridentate ligand was shown via spectroscopic methods to generate transiently stable high-valent Pd^{III} and Pd^{IV} centers. As a result, the corresponding aerobically induced reactivity of the $(^{\mathrm{TsMe}}\mathrm{N4})\mathrm{Pd^{II}Me_2}$ complex was improved by favoring the direct formation of the key $[(^{\mathrm{TsMe}}\mathrm{N4})\mathrm{Pd^{IV}Me_3}]^+$ intermediate which in turn undergoes faster reductive elimination to cleanly

Scheme 7. Proposed Mechanism for the Aerobic Oxidation of (^{TsMe}N4)Pd^{II}Me$_2$ (3) and Subsequent Ethane Formation
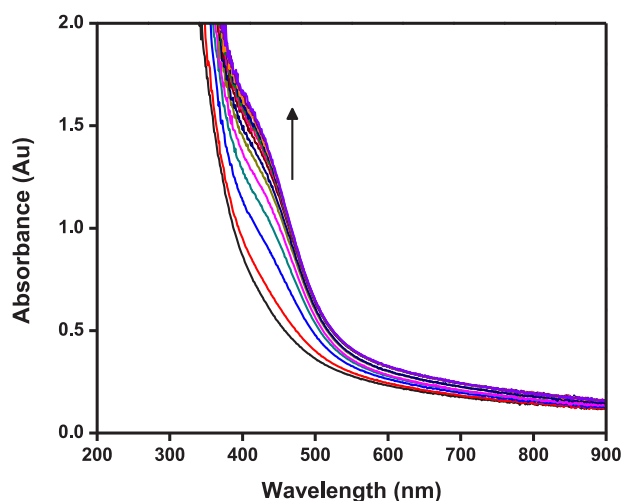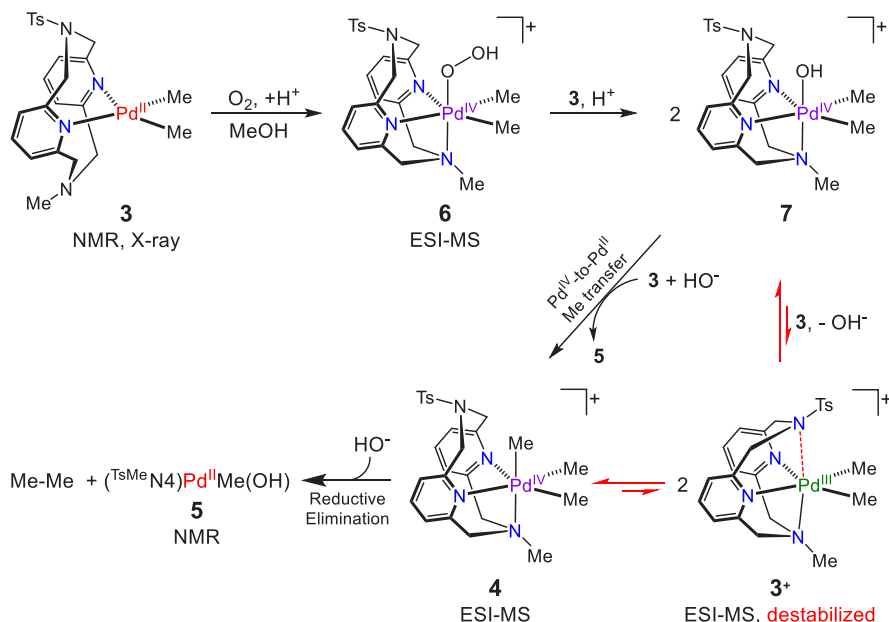
Figure 7. UV−vis spectrum of a 2.14 mM solution of (^{TsMe}N4)PdMe$_2$ in MeOH under O$_2$ at 20 °C (t = 0−26 h, spectra collected every 2 h), showing the growth of the absorption band at 440 nm, without any intermediate species being observed.

generate a stoichiometric amount of ethane without the formation of any methane side product. Overall, these results suggest that finely tuning the donating ability of the donor atoms as well as the denticity of the multidentate ligand employed can improve the aerobically induced reactivity of the Pd^{II} complexes via transient high-valent Pd intermediates to generate cleanly the reductive elimination products and thus has the potential to be further developed into catalytic oxidative transformations.

■ EXPERIMENTAL DETAILS

General Specifications. All manipulations were carried out under a nitrogen atmosphere using standard Schlenk and glovebox techniques if not indicated otherwise. All reagents for which synthesis is not given were commercially available from Aldrich, Acros, STREM, or Pressure Chemical and were used as received without further purification. Solvents were purified prior to use by passing

through a column of activated alumina using an MBRAUN SPS. 2,11-Diaza[3.3](2,6)pyridinophane (N$_4$H$_2$),[34] (COD)PdCl$_2$,[36] (COD)-PdMeCl,[37] and (COD)PdMe$_2$[18] were prepared according to the literature procedures. ^{1}H NMR spectra were recorded on a Varian Mercury-300 spectrometer (300.121 MHz) or Varian Unity Inova-600 spectrometer (599.746 MHz). ^{13}C NMR spectra were recorded on a Varian Unity Inova-600 spectrometer (599.746 MHz). UV−visible spectra were recorded on a Varian Cary 50 Bio spectrophotometer and are reported as λ_{max}, nm (ε, M^{-1} cm^{-1}). EPR spectra were recorded on a JEOL JES-FA X-band (9.2 GHz) EPR spectrometer in frozen solution at 77 K. ESI-MS experiments were performed using a Thermo FT or Bruker Maxis Q-TOF mass spectrometer with an electrospray ionization source. Elemental analyses were carried out by the Columbia Analytical Services Tucson Laboratory. Cyclic voltammetry experiments were performed with a BASi EC Epsilon electrochemical workstation or a CHI 660D electrochemical analyzer. Electrochemical-grade (Bu$_4$N)ClO$_4$ from Fluka was used as the supporting electrolyte. Electrochemical measurements were performed under a blanket of nitrogen, and the analyzed solutions were deaerated by purging with nitrogen. A glassy carbon disk electrode (d = 1.6 mm) was used as the working electrode for cyclic voltammetry. The auxiliary electrode was a Pt wire for cyclic voltammetry measurements. The nonaqueous Ag wire reference electrode assembly was filled with 0.01 M AgNO$_3$/0.1 M (Bu$_4$N)-ClO$_4$/MeCN solution. The reference electrodes were calibrated against Cp$_2$Fe (Fc).

Preparation and Isolation of ^{TsH}N4. Solid N$_4$H$_2$ (1.67g, 6.95 mmol) was placed in a 1000 mL round-bottom flask equipped with a magnetic stirring bar and dissolved in 200 mL of dry CH$_2$Cl$_2$. Then triethylamine (970 μL, 6.95 mmol) was added. The resulting solution was cooled down to 0 °C under nitrogen atmosphere. And a solution of p-toluenesulfonyl chloride (1.325 g, 6.95 mmol) in 400 mL of dry CH$_2$Cl$_2$ was added dropwise. After the addition was complete, the reaction was stirred at 0 °C for an additional 3 h. After the reaction was complete, the reaction mixture was washed with a solution of saturated sodium bicarbonate (3 × 200 mL). The organic layer was then dried over potassium carbonate for 30 min and concentrated to dryness to isolate a product mixture of ^{TsH}N4 and N$_4$Ts$_2$. The product mixture was then suspended in 600 mL of isopropanol. The suspension was stirred overnight and then vacuum filtered. The solid and filtrate were dried separately resulting in N$_4$Ts$_2$ (1.14 g, 2.08 mmol) and ^{TsH}N4 (1.28 g, 3.24 mmol, 47%) respectively. ^{1}H NMR (300 MHz, CDCl$_3$), δ (ppm): 7.83 (d, 2H, Ts-H), 7.41 (d, 2H, Ts-

H), 7.22 (t, 2H, Py-H), 7.10 (d, 2H, Py-H), 6.64 (d, 2H, Py-H), 4.52 (s, 4H, $-CH_2-$), 3.96 (s, 4H, $-CH_2-$), and 2.46 (s, 3H, $-CH_3$). ^{13}C NMR (600 MHz, CDCl$_3$), δ (ppm): 158.60, 155.31, 143.60, 136.37, 129.94, 126.91, 122.06, 120.88, 57.16, 55.75, 21.54. ESI-MS of $[^{TsH}N4H]^+$ in acetonitrile: m/z 395.1535; calculated: m/z 395.1463.

Preparation of ^{TsMe}N4. Solid ^{TsH}N4 (1.28g, 3.24 mmol) was placed in a 500 mL round-bottom flask equipped with a magnetic stirring bar and dissolved in 200 mL of concentrated formic acid and 20 mL of 40% formaldehyde solution. The solution was stirred and refluxed at 110 °C for 24 h under nitrogen atmosphere. The solution was then treated with 20 mL of concentrated hydrochloric acid. After several minutes, the solution was concentrated to dryness. The residue was basified with 1 M sodium hydroxide solution and extracted with CH$_2$Cl$_2$ (4 × 200 mL). The combined organic portions were dried over anhydrous potassium carbonate and filtered. The filtrate was concentrated to dryness resulting in a yellow-white solid, ^{TsMe}N4 (1.145g, 2.82 mmol, 87%). ^{1}H NMR (300 MHz, CDCl3), δ (ppm): 7.78 (d, 2H, Ts-H), 7.40 (d, 2H, Ts-H), 7.23 (t, 2H, Py-H), 7.10 (d, 2H, Py-H), 6.86 (d, 2H, Py-H), 4.52 (s, 4H, $-CH_2-$), 3.80 (s, 4H, $-CH_2-$), 2.72 (s, 3H, $-CH_3$), 2.49 (s, 3H, $-CH_3$). ^{13}C NMR (600 MHz, CDCl3), δ (ppm): 157.16, 154.55, 143.56, 136.33, 135.99, 129.91, 126.86, 123.20, 122.53, 65.73, 56.56, 49.04, 21.49. ESI-MS in acetonitrile: m/z 409.1695; calculated: m/z 409.1620.

Synthesis of ^{TsMe}N4PdCl$_2$ (1). Solid samples of (COD)PdCl$_2$ (71.1 mg, 2.50 mmol) and ^{TsMe}N4 (102.3 mg, 2.50 mmol) were placed into 100 mL round-bottom flask equipped with a magnetic stirring bar and a septum. The flask was evacuated and refilled with nitrogen three times. Then 60 mL of anhydrous CH$_2$Cl$_2$ was added with a syringe and the reaction mixture was stirred vigorously under nitrogen for 2 days in the dark. Using an ice-bath, the CH$_2$Cl$_2$ was rotary evaporated, leaving an orange precipitate. The precipitate was redissolved in the minimal amount of dichloromethane and precipitated with the addition of excess diethyl ether. The precipitated was filtered off, washed with ether, pentane, and dried under a vacuum. The resulting precipitation was a pale orange-brown solid (0.1250 g, 2.13 mmol, 86%). ^{1}H NMR (600 MHz, DMSO), δ (ppm) for *Major Isomer 1′ ($N_{py}N_{am}Pd^{II}Cl_2$)*: 8.00 (d, 2H, Ts-H), 7.96 (t, 2H, Py-H), 7.56 (m, 6H, Ts-H & Py-H), 6.25 (dd, 4H, $-CH_2-$), 5.50 (d, 2H, $-CH_2-$), 4.53 (d, 2H, $-CH_2-$), 2.47 (s, 3H, $-CH_3$), 2.22 (s, 3H, $-CH_3$). ^{1}H NMR (600 MHz, DMSO), δ (ppm) for *Minor Isomer 1″ ($N_{py}N_{py}Pd^{II}Cl_2$)*: 7.90 (d, 2H, Ts-H), 7.66 (t, 2H, Py-H), 7.55 (d, 2H, Ts-H), 7.26 (d, 2H, Py-H), 7.14 (d, 2H, Py-H), 5.22 (d, 2H, $-CH_2-$), 5.15 (d, 2H, $-CH_2-$) 4.66 (d, 2H, $-CH_2-$), 3.96 (d, 2H, $-CH_2-$), 3.03 (s, 3H, $-CH_3$), 2.47 (s, 3H, $-CH_3$). ESI-MS: m/z 549.0; Calculated for $[(^{TsMe}N4)PdCl]^+$: m/z 549.0. Anal. Found: C, 42.77; H, 3.52; N, 8.59. Calcd for C$_{22}$H$_{24}$Cl$_2$N$_4$O$_2$Pd$_2$S·1/2CH$_2$Cl$_2$: C, 43.01; H, 4.01; N, 8.92.

Synthesis of ^{TsMe}N4PdMeCl (2). Solid samples of (COD)-PdMeCl (63.7 mg, 2.40 mmol) and ^{TsMe}N4 (98.2 mg, 2.40 mmol) were placed into 100 mL round-bottom flask equipped with a magnetic stirring bar and a septum. The flask was evacuated and refilled with nitrogen three times. Then 40 mL of anhydrous ether was added with a syringe, and the reaction mixture was stirred vigorously under nitrogen for 2 days in the dark. Pale gray precipitate was filtered off, washed with ether, pentane, and dried under a vacuum. The solid was dissolved in a minimal amount of dichloromethane and precipitated with the addition of excess pentane. The precipitate was a pale gray solid (114.2 mg, 2.02 mmol, 84%). ^{1}H NMR (300 MHz, CDCl3), δ (ppm): 7.84 (d, 2H, Ts-H), 7.52 (m, 4H, Py-H), 7.44 (d, 2H, Ts-H), 7.06 (dd, 2H, Py-H), 6.15 (m, 4H, $-CH_2-$), 5.18 (dd, 2H, $-CH_2-$), 4.24 (dd, 2H, $-CH_2-$), 2.53 (s, 3H, $-CH_3$), 2.34 (s, 3H, $-CH_3$), 1.62 (s, 3H, Pd-CH$_3$). ^{13}C NMR (600 MHz, CDCl3), δ (ppm): 158.30, 157.00, 144.41, 138.19, 136.39, 130.33, 126.79, 125.34, 125.01, 66.02, 63.43, 59.66, 57.41, 39.52, 21.59, −6.92. ESI-MS: m/z 529.1; Calculated for $[(^{TsMe}N4)PdMe]^+$: m/z 529.1. Anal. Found: C, 44.31; H, 4.19; N, 8.47. Calcd for C$_{23}$H$_{27}$ClN$_4$O$_2$Pd$_2$S (CH$_2$Cl$_2$): C, 44.32; H, 4.49; N, 8.61.

Synthesis of ^{TsMe}N4PdMe$_2$ (3). Solid samples of (COD)PdMe$_2$ (0.3740 g, 1.52 mmol) and ^{TsMe}N4 (0.6227 g, 1.52 mmol) were cooled down to 0 °C in an ice bath, and then the flask was evacuated/

refilled with nitrogen three times. Then under nitrogen, 30 mL of anhydrous ether was added. The reaction mixture was stirred vigorously at 0 °C for 3 h, and then the solvents were removed by evaporation on a high vacuum line at 0 °C. The resulting pale yellow-white solid was transported under nitrogen into the glovebox. The solid was washed with pentane and then dissolved in a minimal amount of tetrahydrofuran. The resulting orange-colored solution was precipitated with pentane. The cloudy solution was then decanted, and the solid was dried under a vacuum, resulting in a pale yellow-orange solid (0.4889 g, 0.90 mmol, 59%). ^{1}H NMR (300 MHz, benzene), δ (ppm) for *Major Isomer 1′ ($N_{py}N_{py}Pd^{II}Me_2$)*: 7.65 (d, 2H, Ts-H), 7.34 (d, 2H, Ts-H), 6.81 (d, 2H, Py-H), 6.66 (t, 2H, Py-H), 6.37 (m, 4H, $-CH2-$), 6.22 (d, 2H, Py-H), 4.83 (d, 2H, $-CH_2-$), 3.68 (d, 2H, $-CH_2-$), 1.97 (s, 3H, $-CH3$), 1.95 (s, 3H, $-CH3$), 0.84 (s, 6H, Pd-CH3). ^{1}H NMR (300 MHz, Benzene), δ (ppm) for *Minor Isomer 1″ ($N_{py}N_{am}Pd^{II}Me_2$)*: 7.57 (d, 2H, Ts-H), 7.39 (d, 2H, Ts-H), 7.25 (m, 2H, Py-H), 6.55 (t, 2H, Py-H), 6.04 (m, 2H, Py), 5.28 (d, 1H, $-CH_2-$), 4.74 (dd, 2H, $-CH2-$), 3.86 (d, 1H, $-CH2-$), 1.97 (s, 3H, $-CH3$), 1.95 (s, 3H, $-CH3$), 0.70 (d, 6H, Pd-CH3). ^{13}C NMR (600 MHz, benzene), δ (ppm): 157.86, 157.45, 143.27, 138.10, 136.61, 130.11, 128.30, 127.05, 124.47, 63.66, 57.46, 39.57, 21.21, and −9.45. ESI-MS: m/z 529.1; calculated for $[(^{TsMe}N4)PdMe]^+$: m/z 529.1. The elemental analysis of this complex could not be obtained due to its high air sensitivity.

General Procedure for the Oxidation of 3 with O$_2$. A 3–4 mM solution of **3** with an equimolar amount of 1,3,5-trimethoxybenzene (used as internal standard) was dissolved in O$_2$-saturated CD$_3$OD solution, and an NMR tube was filled to the top (to avoid the escape of volatiles into the headspace) and sealed with a septum. The reaction mixture was kept in the dark and periodically analyzed by ^{1}H NMR. The yields of Pd intermediates and organic/Pd products were determined by integration versus the internal standard, calculated as [moles of product]/[moles of **3**]*100% and given as an average of two runs.

UV−vis Studies of Oxidation of 3 with O$_2$. A ~2 mM solution of **3** in MeOH was placed into a quartz cuvette (path length 1.0 cm) equipped with a septum-sealed cap and a magnetic stir bar. Oxygen was bubbled through the solution for 2−3 min, and the reaction mixture was stirred under O$_2$ at 20 °C in the dark. The reaction progress was then monitored by UV−vis.

ESI-MS Studies of Oxidation of 3 with O$_2$. A ~0.2 mM solution of **3** in 1 mL of O$_2$-saturated MeOH was prepared, and then ~50 μL of solution was injected into the MS instrument at various time points to detect any transient intermediates present in the reaction mixture.

X-ray Structure Determination of 1, 2, and 3. Suitable crystals were mounted on Mitgen cryoloops in random orientations in a Bruker Kappa Apex-II CCD X-ray diffractometer equipped with an Oxford Cryostream LT device and a fine focus Mo Kα radiation X-ray source (λ = 0.71073 Å). Preliminary unit cell constants were determined with a set of 36 narrow frame scans. Typical data sets consist of combinations of ϕ and ϕ scan frames with a typical scan width of 0.5° and a counting time of 15−30 s/frame at a crystal-to-detector distance of ~4.0 cm. The collected frames were integrated using an orientation matrix determined from the narrow frame scans. Apex II and SAINT software package[51] were used for data collection and data integration. Analysis of the integrated data did not show any decay. Final cell constants were determined by global refinement of xyz centroids of reflections from the complete data sets. Collected data were corrected for systematic errors using SADABS[52] based on the Laue symmetry using equivalent reflections. Structure solutions and refinement were carried out using the SHELXTL-PLUS software package.[52] The structures were refined with full matrix least-squares refinement by minimizing $\sum w(F_o^2 - F_c^2)^2$. All non-hydrogen atoms were refined anisotropically to convergence, and the hydrogen atoms were added at the calculated positions in the final refinement cycles. Crystal data and intensity data collection parameters are listed in Tables S8−S13.

Computational Studies. The density functional theory (DFT) and time-dependent density functional theory (TD-DFT) calculations

were performed with the program package Gaussian 09.[53] The UB3LYP hybrid functional[54,55] along with the Stevens (CEP-31G)[56,57] valence basis sets and effective core potentials were employed. This combination of hybrid functional and basis sets have been previously shown to work well for reproducing experimental parameters of Pd complexes.[58,59] The ground state wave function was investigated by analyzing the frontier MOs, and the atomic contributions to MOs were calculated using the program Chemissian.[60] TD-DFT calculations were employed to obtain the predicted absorption bands and their major contributing transitions. The calculated UV–vis spectra were generated using GaussSum,[61] with a full width at half maximum (fwhm) values of 3500 and 3000 cm^{-1} for complexes $[(^{TsMe}N4)Pd^{III}Cl_2]^+$ (**1$^+$**) and $[(^{TsMe}N4)Pd^{III}MeCl]^+$ (**2$^+$**) respectively.

■ ASSOCIATED CONTENT

Ⓢ Supporting Information

The Supporting Information is available free of charge at https://pubs.acs.org/doi/10.1021/acs.inorgchem.0c01763.

> Detailed experimental details, spectroscopic characterization, aerobic oxidation studies, computational details, and X-ray crystallographic data (PDF)

Accession Codes

CCDC 2009613−2009615 contain the supplementary crystallographic data for this paper. These data can be obtained free of charge via www.ccdc.cam.ac.uk/data_request/cif, or by emailing data_request@ccdc.cam.ac.uk, or by contacting The Cambridge Crystallographic Data Centre, 12 Union Road, Cambridge CB2 1EZ, UK; fax: +44 1223 336033.

■ AUTHOR INFORMATION

Corresponding Author

Liviu M. Mirica − *Department of Chemistry, University of Illinois at Urbana-Champaign, Urbana, Illinois 61801, United States;* ⓞ orcid.org/0000-0003-0584-9508; Email: mirica@illinois.edu

Authors

Jason W. Schultz − *Department of Chemistry, Washington University, St. Louis, Missouri 63130, United States*

Nigam P. Rath − *Department of Chemistry and Biochemistry, One University Boulevard, University of Missouri, St. Louis, Missouri 63121, United States*

Complete contact information is available at:
https://pubs.acs.org/10.1021/acs.inorgchem.0c01763

Notes

The authors declare no competing financial interest.

■ ACKNOWLEDGMENTS

■ REFERENCES

(1) Stoltz, B. M. Palladium catalyzed aerobic dehydrogenation: from alcohols to indoles and asymmetric catalysis. *Chem. Lett.* **2004**, *33*, 362−367.

(2) Stahl, S. S. Palladium oxidase catalysis. Selective oxidation of organic chemicals by direct dioxygen-coupled turnover. *Angew. Chem., Int. Ed.* **2004**, *43*, 3400−3420.

(3) Stahl, S. S. Palladium-catalyzed oxidation of organic chemicals with O₂. *Science* **2005**, *309*, 1824−1826.

(4) Beck, E. M.; Grimster, N. P.; Hatley, R.; Gaunt, M. J. Mild Aerobic Oxidative Palladium (II) Catalyzed C-H Bond Functionaliza-

tion: Regioselective and Switchable C-H Alkenylation and Annulation of Pyrroles. *J. Am. Chem. Soc.* **2006**, *128*, 2528−2529.

(5) Sigman, M. S.; Jensen, D. R. Ligand-Modulated Palladium-Catalyzed Aerobic Alcohol Oxidations. *Acc. Chem. Res.* **2006**, *39*, 221−229.

(6) Gligorich, K. M.; Sigman, M. S. Recent advancements and challenges of palladium(II)-catalyzed oxidation reactions with molecular oxygen as the sole oxidant. *Chem. Commun.* **2009**, 3854−3867.

(7) Campbell, A. N.; Stahl, S. S. Overcoming the "Oxidant Problem": Strategies to Use O₂ as the Oxidant in Organometallic C-H Oxidation Reactions Catalyzed by Pd (and Cu). *Acc. Chem. Res.* **2012**, *45*, 851−863.

(8) Shi, Z.; Zhang, C.; Tang, C.; Jiao, N. Recent advances in transition-metal catalyzed reactions using molecular oxygen as the oxidant. *Chem. Soc. Rev.* **2012**, *41*, 3381−3430.

(9) Canty, A. J. Development of organopalladium(IV) chemistry: fundamental aspects and systems for studies of mechanism in organometallic chemistry and catalysis. *Acc. Chem. Res.* **1992**, *25*, 83−90.

(10) Canty, A. J. Organopalladium and platinum chemistry in oxidising milieu as models for organic synthesis involving the higher oxidation states of palladium. *J. Chem. Soc., Dalton Trans.* **2009**, 10409−17.

(11) Zhang, J.; Khaskin, E.; Anderson, N. P.; Zavalij, P. Y.; Vedernikov, A. N. Catalytic aerobic oxidation of substituted 8-methylquinolines in PdII-2,6-pyridinedicarboxylic acid systems. *Chem. Commun.* **2008**, 3625−3627.

(12) Zhang, Y.-H.; Yu, J.-Q. Pd(II)-Catalyzed Hydroxylation of Arenes with 1 atm of O₂ or Air. *J. Am. Chem. Soc.* **2009**, *131*, 14654−14655.

(13) Wang, A.; Jiang, H.; Chen, H. Palladium-Catalyzed Diacetoxylation of Alkenes with Molecular Oxygen as Sole Oxidant. *J. Am. Chem. Soc.* **2009**, *131*, 3846−3847.

(14) Boisvert, L.; Denney, M. C.; Hanson, S. K.; Goldberg, K. I. Insertion of Molecular Oxygen into a Palladium(II) Methyl Bond: A Radical Chain Mechanism Involving Palladium(III) Intermediates. *J. Am. Chem. Soc.* **2009**, *131*, 15802−15814.

(15) Zhu, M.-K.; Zhao, J.-F.; Loh, T.-P. Palladium-Catalyzed Oxime Assisted Intramolecular Dioxygenation of Alkenes with 1 atm of Air as the Sole Oxidant. *J. Am. Chem. Soc.* **2010**, *132*, 6284−6285.

(16) Vedernikov, A. N. Direct Functionalization of M-C (M = PtII, PdII) Bonds Using Environmentally Benign Oxidants, O2 and H2O2. *Acc. Chem. Res.* **2012**, *45*, 803−813.

(17) Sberegaeva, A. V.; Zavalij, P. Y.; Vedernikov, A. N. Oxidation of a Monomethylpalladium(II) Complex with O2 in Water: Tuning Reaction Selectivity to Form Ethane, Methanol, or Methylhydroperoxide. *J. Am. Chem. Soc.* **2016**, *138*, 1446−1455.

(18) Khusnutdinova, J. R.; Rath, N. P.; Mirica, L. M. The Aerobic Oxidation of a Pd(II) Dimethyl Complex Leads to Selective Ethane Elimination from a Pd(III) Intermediate. *J. Am. Chem. Soc.* **2012**, *134*, 2414−2422.

(19) Tang, F.; Zhang, Y.; Rath, N. P.; Mirica, L. M. Detection of Pd(III) and Pd(IV) Intermediates during the Aerobic Oxidative C-C Bond Formation from a Pd(II) Dimethyl Complex. *Organometallics* **2012**, *31*, 6690−6696.

(20) Khusnutdinova, J. R.; Qu, F.; Zhang, Y.; Rath, N. P.; Mirica, L. M. Formation of the Palladium(IV) Complex [(Me3tacn)-PdIVMe3]+ through Aerobic Oxidation of (Me3tacn)PdIIMe2 (Me3tacn = N,N′,N″-Trimethyl-1,4,7-triazacyclononane). *Organometallics* **2012**, *31*, 4627−4630.

(21) Mirica, L. M.; Khusnutdinova, J. R. Structure and Electronic Properties of Pd(III) Complexes. *Coord. Chem. Rev.* **2013**, *257*, 299−314.

(22) Khusnutdinova, J. R.; Mirica, L. M., Organometallic Pd(III) Complexes in C-C and C-Heteroatom Bond Formation Reactions. In *C-H and C-X Bond Functionalization: Transition Metal Mediation*; Ribas, X., Ed.; Royal Society of Chemistry: 2013; pp 122−158.

(23) Wessel, A. J.; Schultz, J. W.; Tang, F.; Duan, H.; Mirica, L. M. Improved synthesis of symmetrically & asymmetrically N-substituted pyridinophane derivatives. *Org. Biomol. Chem.* **2017**, *15*, 9923−9931.

(24) Smith, S. M.; Planas, O.; Gomez, L.; Rath, N.; Ribas, X.; Mirica, L. M. Aerobic C-C and C-O bond formation reactions mediated by high-valent nickel species. *Chem. Sci.* **2019**, *10*, 10366−10372.

(25) Smith, S. M.; Rath, N. P.; Mirica, L. M. Axial Donor Effects on Oxidatively Induced Ethane Formation from Nickel-Dimethyl Complexes. *Organometallics* **2019**, *38*, 3602−3609.

(26) Tang, F. Z.; Qu, F. R.; Khusnutdinova, J. R.; Rath, N. P.; Mirica, L. M. Structural and reactivity comparison of analogous organometallic Pd(III) and Pd(IV) complexes. *Dalton Trans.* **2012**, *41*, 14046−14050.

(27) Mirica, L. M.; Khusnutdinova, J. R. Structure and electronic properties of Pd(III) complexes. *Coord. Chem. Rev.* **2013**, *257*, 299−314.

(28) Tang, F. Z.; Park, S. V.; Rath, N. P.; Mirica, L. M. Electronic versus steric effects of pyridinophane ligands on Pd(III) complexes. *Dalton Trans.* **2018**, *47*, 1151−1158.

(29) Zhou, W.; Watson, M. B.; Zheng, S.; Rath, N. P.; Mirica, L. M. Ligand effects on the properties of Ni(III) complexes: aerobically-induced aromatic cyanation at room temperature. *Dalton Trans.* **2016**, *45*, 15886−15893.

(30) Zhou, W.; Zheng, S. A.; Schultz, J. W.; Rath, N. P.; Mirica, L. M. Aromatic Cyanoalkylation through Double C-H Activation Mediated by Ni(III). *J. Am. Chem. Soc.* **2016**, *138*, 5777−5780.

(31) Kim, J.; Shin, B.; Kim, H.; Lee, J.; Kang, J.; Yanagisawa, S.; Ogura, T.; Masuda, H.; Ozawa, T.; Cho, J. Steric Effect on the Nucleophilic Reactivity of Nickel(III) Peroxo Complexes. *Inorg. Chem.* **2015**, *54*, 6176−6183.

(32) Xu, S.; Bucinsky, L.; Breza, M.; Krzystek, J.; Chen, C. H.; Pink, M.; Telser, J.; Smith, J. M. Ligand Substituent Effects in Manganese Pyridinophane Complexes: Implications for Oxygen-Evolving Catalysis. *Inorg. Chem.* **2017**, *56*, 14315−14325.

(33) Khusnutdinova, J. R.; Rath, N. P.; Mirica, L. M. Stable Mononuclear Organometallic Pd(III) Complexes and Their C-C Bond Formation Reactivity. *J. Am. Chem. Soc.* **2010**, *132*, 7303−7305.

(34) Bottino, F.; Di Grazia, M.; Finocchiaro, P.; Fronczek, F. R.; Mamo, A.; Pappalardo, S. Reaction of Tosylamide Monosodium Salt with Bis(halomethyl) Compounds: an Easy Entry to Symmetrical N-tosylazamacrocycles. *J. Org. Chem.* **1988**, *53*, 3521−9.

(35) Tang, F.; Qu, F.; Khusnutdinova, J. R.; Rath, N. P.; Mirica, L. M. Structural and Reactivity Comparison of Analogous Organometallic Pd(III) and Pd(IV) Complexes. *Dalton Trans.* **2012**, *41*, 14046−14050.

(36) Drew, D.; Doyle, J. R.; Shaver, A. G. Cyclic diolefin complexes of platinum and palladium. *Inorg. Synth.* **2007**, *28*, 346−349.

(37) Rulke, R. E.; Ernsting, J. M.; Spek, A. L.; Elsevier, C. J.; van Leeuwen, P. W. N. M.; Vrieze, K. NMR study on the coordination behavior of dissymmetric terdentate trinitrogen ligands on methylpalladium(II) compounds. *Inorg. Chem.* **1993**, *32*, 5769.

(38) Khusnutdinova, J. R.; Rath, N. P.; Mirica, L. M. The Conformational Flexibility of the Tetradentate Ligand ^{tBu}N4 is Essential for the Stabilization of (^{tBu}N4)Pd^{III} Complexes. *Inorg. Chem.* **2014**, *53*, 13112−13129.

(39) See Supporting Information.

(40) Byers, P. K.; Canty, A. J.; Skelton, B. W.; White, A. H. The Oxidative Addition of Iodomethane to [PdMe2(2,2'-bipyridyl)] and the X-ray Structure of the Organopalladium(IV) Product fac-[PdMe3(2,2'-bipyridyl)L]. *J. Chem. Soc., Chem. Commun.* **1986**, *0*, 1722−1724.

(41) Byers, P. K.; Canty, A. J.; Skelton, B. W.; White, A. H. Synthesis of the 1st Organopalladium(IV) Cations, Including the 1st X-ray Study of Isostructural Organopalladium(IV) and Platinum(IV) Complexes, [fac-MMe3(tris(pyrazol-1-yl)methane-N,N',N'')]I. *J. Chem. Soc., Chem. Commun.* **1987**, 1093−1095.

(42) Byers, P. K.; Canty, A. J.; Skelton, B. W.; White, A. H. Synthesis, reactivity, and structural studies in trimethylpalladium(IV) chemistry, including PdIMe3(bpy) and [MMe3((pz)3CH)]+ (M = palladium, platinum). *Organometallics* **1990**, *9*, 826−832.

(43) Canty, A. J.; Honeyman, R. T.; Roberts, A. S.; Traill, P. R.; Colton, R.; Skelton, B. W.; White, A. H. Oxidation of organoplatinum(II) and -palladium(II) complexes by water. The X-ray structure of the trimethylpalladium(IV) complex fac-[PdMe3-{tris(pyrazol-1-yl)borate}] formed on oxidation of a dimethylpalladium(II) reagent. *J. Organomet. Chem.* **1994**, *471*, C8−C10.

(44) Canty, A. J.; Jin, H.; Roberts, A. S.; Skelton, B. W.; Traill, P. R.; White, A. H. Synthesis and Characterization of Ambient Temperature Stable Organopalladium(IV) Complexes, Including Aryl-, .eta.1-Allyl-, Ethylpalladium(IV), and Pallada(IV)cyclopentane Complexes. Structures of the Poly(pyrazol-1-yl)borate Complexes PdMe3{(pz)3BH} and PdMe3{(pz)4B} and Three Polymorphs of PdMe2Et{(pz)3BH}. *Organometallics* **1995**, *14*, 199−206.

(45) Canty, A. J.; Dedieu, A.; Jin, H.; Milet, A.; Skelton, B. W.; Trofimenko, S.; White, A. H. Coordination geometries for palladium and platinum: theoretical studies and the synthesis and structure of tris(indazol-1-yl)borate complexes MMe3{(ind)3BH}. *Inorg. Chim. Acta* **1999**, *287*, 27−36.

(46) Bayler, A.; Canty, A. J.; Edwards, P. G.; Skelton, B. W.; White, A. H. Trimethyl-palladium(IV) and -platinum(IV) complexes containing phosphine donor ligands, including studies of 1,5,9-triethyl-1,5,9-triphosphacyclodecane and X-ray structural studies of palladium(II) and palladium(IV) complexes. *Dalton Trans.* **2000**, 3325−3330.

(47) Rostovtsev, V. V.; Henling, L. M.; Labinger, J. A.; Bercaw, J. E. Structural and mechanistic investigations of the oxidation of dimethylplatinum(II) complexes by dioxygen. *Inorg. Chem.* **2002**, *41*, 3608−3619.

(48) Prokopchuk, E. M.; Puddephatt, R. J. Dimethylplatinum(IV) chemistry: Stannyl, hydride, hydroxide, and aqua complexes. *Can. J. Chem.* **2003**, *81*, 476−483.

(49) Prokopchuk, E. M.; Jenkins, H. A.; Puddephatt, R. J. Stable Cationic Dimethyl(hydrido)platinum(IV) Complex. *Organometallics* **1999**, *18*, 2861−2866.

(50) Powers, D. C.; Lee, E.; Ariafard, A.; Sanford, M. S.; Yates, B. F.; Canty, A. J.; Ritter, T. Connecting Binuclear Pd(III) and Mononuclear Pd(IV) Chemistry by Pd-Pd Bond Cleavage. *J. Am. Chem. Soc.* **2012**, *134*, 12002−12009.

(51) Bruker Analytical X-Ray: Madison, WI, 2008.

(52) Sheldrick, G. M. A short history of SHELX. *Acta Crystallogr., Sect. A: Found. Crystallogr.* **2008**, *64*, 112−122.

(53) Frisch, M. J.; Trucks, G. W.; Schlegel, H. B.; Scuseria, G. E.; Robb, M. A.; Cheeseman, J. R.; Scalmani, G.; Barone, V.; Mennucci, B.; Petersson, G. A.; Nakatsuji, H.; Caricato, M.; Li, X.; Hratchian, H. P.; Izmaylov, A. F.; Bloino, J.; Zheng, G.; Sonnenberg, J. L.; Hada, M.; Ehara, M.; Toyota, K.; Fukuda, R.; Hasegawa, J.; Ishida, M.; Nakajima, T.; Honda, Y.; Kitao, O.; Nakai, H.; Vreven, T.; Montgomery, J. A., Jr.; Peralta, J. E.; Ogliaro, F.; Bearpark, M.; Heyd, J. J.; Brothers, E.; Kudin, K. N.; Staroverov, V. N.; Kobayashi, R.; Normand, J.; Raghavachari, K.; Rendell, A.; Burant, J. C.; Iyengar, S. S.; Tomasi, J.; Cossi, M.; Rega, N.; Millam, J. M.; Klene, M.; Knox, J. E.; Cross, J. B.; Bakken, V.; Adamo, C.; Jaramillo, J.; Gomperts, R.; Stratmann, R. E.; Yazyev, O.; Austin, A. J.; Cammi, R.; Pomelli, C.; Ochterski, J. W.; Martin, R. L.; Morokuma, K.; Zakrzewski, V. G.; Voth, G. A.; Salvador, P.; Dannenberg, J. J.; Dapprich, S.; Daniels, A. D.; Farkas, O.; Foresman, J. B.; Ortiz, J. V.; Cioslowski, J.; Fox, D. J., *Gaussian 09*, Revision A.02; Gaussian, Inc.: Wallingford, CT, 2009.

(54) Becke, A. D. A New Mixing of Hartree-Fock and Local Densisty-Functional Theories. *J. Chem. Phys.* **1993**, *98*, 1372−1377.

(55) Lee, C. T.; Yang, W. T.; Parr, R. G. Development of the Colle-Salvetti Correlation-Energy Formula into a Functional of the Electron-Density. *Phys. Rev. B: Condens. Matter Mater. Phys.* **1988**, *37*, 785−789.

(56) Stevens, W. J.; Basch, H.; Krauss, M. Compact Effective Potentials and Efficient Shared-Exponent Basis-Sets for the 1st-row and 2nd-row Atoms. *J. Chem. Phys.* **1984**, *81*, 6026−6033.

(57) Stevens, W. J.; Krauss, M.; Basch, H.; Jasien, P. G. Relativistic Compact Effective Potentials and Efficient, Shared-Exponent Basis-Sets for the 3rd-row, 4th-row, and 5th-row Atoms. *Can. J. Chem.* **1992**, *70*, 612−630.

(58) Foley, N. A.; Lail, M.; Lee, J. P.; Gunnoe, T. B.; Cundari, T. R.; Petersen, J. L. Comparative reactivity of TpRu(L)(NCMe)Ph (L = CO or PMe3): Impact of ancillary ligand L on activation of carbon-hydrogen bonds including catalytic hydroarylation and hydro-vinylation/oligomerization of ethylene. *J. Am. Chem. Soc.* **2007**, *129*, 6765−6781.

(59) Veige, A. S.; Slaughter, L. M.; Wolczanski, P. T.; Matsunaga, N.; Decker, S. A.; Cundari, T. R. Deoxygenations of (silox)(3)WNO and R3PO by (silox)(3)M (M = V, Ta) and (silox)(3)NbL (silox = (Bu3SiO)-Bu-t): Consequences of electronic effects. *J. Am. Chem. Soc.* **2001**, *123*, 6419−6420.

(60) *Chemissian*, version 4.60, 2018, www.chemissian.com, accessed June 2019.

(61) O'Boyle, N. M.; Tenderholt, A. L.; Langner, K. M. cclib: A library for package-independent computational chemistry algorithms. *J. Comput. Chem.* **2008**, *29*, 839−845.